

# Unconventional superconductivity in YPtBi and related topological semimetals

Markus Meinert<sup>1,\*</sup>

<sup>1</sup>*Center for Spinelectronic Materials and Devices,  
Bielefeld University, D-33501 Bielefeld, Germany*

(Dated: June 19, 2022)

YPtBi, a topological semimetal with very low carrier density, was recently found to be superconducting below  $T_c = 0.77$  K. In the conventional theory, the nearly vanishing density of states around the Fermi level would imply a vanishing electron-phonon coupling and would therefore not allow for superconductivity. Based on relativistic density functional theory calculations of the electron-phonon coupling in YPtBi it is found that carrier concentrations of more than  $10^{21} \text{ cm}^{-3}$  are required to explain the observed critical temperature with the conventional pairing mechanism, which is several orders of magnitude larger than experimentally observed. It is very likely that an unconventional pairing mechanism is responsible for the superconductivity in YPtBi and related topological semimetals with the Half-Heusler structure.

A series of Half-Heusler compounds with heavy elements were predicted to be 3D topological insulators [1] under strain [2–4]. They would exhibit surface states with Dirac-like dispersion, i.e., the electrons behave as massless particles with ultrahigh mobility. These surface states are topologically protected as long as time-reversal symmetry is preserved, i.e., they are protected against scattering from non-magnetic impurities. Most of the Half-Heusler candidates for topological insulators are in fact semimetals with very low density of states (DOS) at the Fermi level  $D(E_F)$ . Nevertheless, for some of these materials there is experimental evidence for topologically nontrivial bandstructures and the presence of Dirac surface states [5–7]. Some compounds from this class were found to be superconductors with critical temperatures up to 1.8 K, e.g. LaPtBi, LuPtBi, LuPdBi, YPtBi, YPdBi [8–12]. Compounds of the type  $RPdBi$  ( $R$  is a lanthanide with an open  $4f$  shell) that show coexisting local moment antiferromagnetism as well as superconductivity were found, pointing to the presence of spin triplet Cooper pairs [12]. The existence of such Cooper pairs with odd-parity wavefunctions (to conserve the total antisymmetry of the Cooper pair wavefunction) is allowed because the missing inversion center of the Half-Heusler structure leads to a coupling of even- and odd-parity pairing wave functions [13]. Due to the topologically nontrivial band structure, novel collective excitations are possible, in particular surface Majorana fermions [14]. These could provide the basis for low-decoherence quantum processing, because the Majorana fermions are protected against most decoherence mechanisms [15].

Superconducting, highly doped semiconductors such as GeTe and SnTe are long known [16, 17] and their superconductivity can be explained [17] with the Eliashberg theory of electron-phonon mediated superconductivity. SrTiO<sub>3-x</sub>, the most dilute semiconductor known to date, has  $T_c \lesssim 0.5$  K and its superconductivity can not be explained by simple electron-phonon coupling [18, 19]. Instead, a plasmon-assisted mechanism was proposed to

explain the unusual dependence of  $T_c$  on the carrier density [20]. From the BCS theory the well-known expression for the superconducting transition temperature  $k_B T_c = 1.13 \hbar \omega_c \exp[-1/D(E_F)V]$  is obtained, where  $\omega_c$  is a cutoff frequency, that is often identified with the Debye frequency, and  $V$  is the effective interaction potential. From free-electron theory, the critical temperature is expected to increase with increasing carrier concentration. This expectation was confirmed for GeTe and SnTe, but in these materials  $T_c$  is limited to a few hundred mK [17]. More recently, superconductivity just below  $T_c \approx 4$  K was also discovered in highly B doped diamond [21] and in Cu<sub>x</sub>Bi<sub>2</sub>Se<sub>3</sub> [22], a prototype topological insulator for  $x = 0$ . For the latter case, it was shown by first principles calculations of the electron-phonon coupling that the conventional pairing mechanism is most likely not strong enough to give rise to the rather high observed critical temperature [23].

Naturally the question arises whether the superconductivity in the topological Half-Heusler compounds is of the conventional, phonon-mediated type. Here, first principles calculations of the electron-phonon coupling for a topological semimetal from the Half-Heusler class are presented. The compound YPtBi was chosen as a representative member of this class, which is a bulk superconductor with a critical temperature of  $T_c = 0.77$  K [9, 24–26]. In this compound the electronic structure is not complicated by the presence of  $f$ -electrons, which allows for efficient and parameter-free quantum mechanical calculations of the electronic and vibrational properties.

The quantity  $D(E_F)V$  occurring in the BCS equation can be split up into a repulsive Coulomb part  $\mu^*$  and an attractive electron-phonon part  $\lambda$ , where  $D(E_F)V = D(E_F)(V_{e-ph} - V_{e-e}) = \lambda - \mu^*$  [27]. The Coulomb pseudo potential  $\mu^*$  is usually taken as a parameter, for which values of  $\mu^* \approx 0.1 - 0.15$  are assumed in conventional metallic semiconductors [27–29]. However, for superconducting highly-doped semiconductors  $\mu^* \rightarrow 0$  seems more appropriate [19]. The critical temperature can be approximately calculated with the McMillan equa-

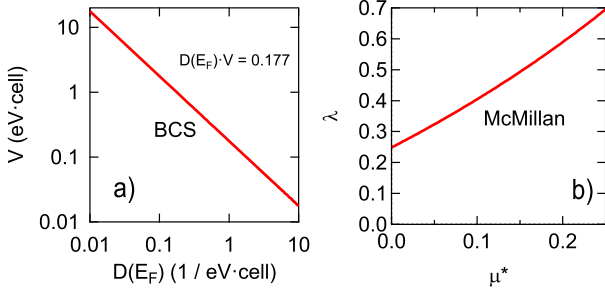


FIG. 1. a): Expected attractive interaction potential  $V$  as a function of the density of states at the Fermi level  $D(E_F)$  based on the BCS equation. b): Electron-phonon coupling constant  $\lambda$  as a function of the retarded repulsive Coulomb pseudo potential  $\mu^*$  obtained from the McMillan equation with  $T_c = 0.77$  K and  $\Theta_D = 195$  K.

tion [30]

$$T_c = \frac{\Theta_D}{1.45} \exp \left[ -\frac{1.04(1 + \lambda)}{\lambda - \mu^*(1 + 0.62\lambda)} \right]. \quad (1)$$

To estimate the interaction  $V$  or  $\lambda$  of YPtBi the Debye temperature  $\Theta_D$  and the density of states  $D(E_F)$  are needed. Both quantities can be extracted from a heat capacity measurement by fitting the low-temperature heat capacity with  $C/T = \gamma + \beta T^2$ . The Sommerfeld coefficient is  $\gamma = \pi^2 D(\varepsilon_F)(1 + \lambda)k_B^2/3$  and  $\beta$  is related to the Debye  $T^3$  law as  $\beta = 12\pi^4 k_B/5\Theta_D^3$ . From the measured values  $\gamma \lesssim 0.1$  mJ/mol K<sup>2</sup> and  $\beta = 0.79(7)$  mJ/mol K<sup>4</sup> one obtains  $\Theta_D = 195(5)$  K and  $D(E_F) \lesssim 0.042$  states/eV cell [31]. These numbers allow the estimate  $V \approx 5$  eV·cell, which is very high. To reproduce the observed  $T_c$ , the lower bound for  $\lambda$  is  $\lambda \geq 0.25$  and assuming  $\mu^* \approx 0.1$  one may expect  $\lambda = 0.41$  based on the McMillan equation, very similar to the coupling in Al or Mo [28].

To shed some light on the relation between the experimentally observed heat capacities, Fermi surfaces and the superconductivity, the electron-phonon interaction of YPtBi was calculated from first-principles based on density functional theory (DFT). To investigate if disorder or off-stoichiometry play a role in the superconductivity, the influence of doping on the electron-phonon coupling was investigated.

The DFT calculations were carried out with the QUANTUM ESPRESSO distribution [32]. Relativistic PAW potentials [33] (including spin-orbit coupling, SOC) from the PSLibrary [34] were employed with kinetic energy cutoffs of 40 Ry for the wavefunctions and 400 Ry for the charge density. The results were checked against all-electron calculations including SOC with the full potential linearized augmented plane-wave (FLAPW) method with the elk code [35] and were found to agree very well. The Perdew-Burke-Ernzerhof (PBE) generalized gradient approximation (GGA) was used for the exchange-

correlation energy and potential. The dynamical matrices and electron-phonon matrix elements  $g_{\mathbf{k}+\mathbf{q},\mathbf{k}}^{\nu,mn}$  with phonon mode index  $\nu$  and band indices  $m, n$  were obtained with density functional perturbation theory on a  $5 \times 5 \times 5$   $\mathbf{q}$ -point mesh and  $10 \times 10 \times 10$   $\mathbf{k}$ -point mesh. Electron-phonon coupling was calculated applying an interpolation scheme described in Ref. 36. The Eliashberg spectral function

$$\alpha^2 F(\omega) = \frac{1}{D(\varepsilon_F)} \sum_{mn} \sum_{\mathbf{q}\nu} \sum_{\mathbf{k}} \delta(\omega - \omega_{\mathbf{q}\nu}) \left| g_{\mathbf{k}+\mathbf{q},\mathbf{k}}^{\nu,mn} \right|^2 \times \delta(\varepsilon_{\mathbf{k}+\mathbf{q},m} - E_F) \delta(\varepsilon_{\mathbf{k},n} - E_F) \quad (2)$$

was evaluated on  $40^3$   $\mathbf{k}$ -point and  $20^3$   $\mathbf{q}$ -point meshes. The electron-phonon coupling constant  $\lambda$  is the first reciprocal moment of the Eliashberg function,

$$\lambda = 2 \int \frac{\alpha^2 F(\omega)}{\omega} d\omega. \quad (3)$$

An extrapolation technique was used to circumvent the very dense  $\mathbf{k}$ -point sampling needed to evaluate the double delta integral defining the spectral function accurately: the spectral function was obtained for several widths of a Gaussian approximation for the  $\delta$ -function between 0.004 and 0.02 Ry. The resulting density of states  $D(E_F)$  and electron-phonon coupling constant  $\lambda$  were extrapolated with a linear fit to the  $\delta \rightarrow 0$  limit. Convergence tests suggest that the accuracy for  $\lambda$  is of the order  $\pm 0.02$  with reasonable computational effort. Doping was treated in a rigid-band approximation by adding or subtracting electrons from the band structure and compensating for this by adding a homogeneous background charge. The experimental lattice constant of 6.65 Å was used in all calculations.

In Figure 2 the DOS, atom-projected DOS, band structure along high-symmetry lines and the Fermi surface are plotted. The relativistic PAW and FLAPW calculations are in excellent agreement, establishing that the PAW method with the potentials from the PSLibrary gives reliable results for YPtBi. The valence band is dominated by Pt 5d states, while the conduction band is governed by Y 4d states. However, due to strong hybridization, all atoms contribute to some extent to any part of the valence and conduction bands, in particular in a range of  $\pm 2$  eV around the Fermi energy. The band structure plot clarifies that YPtBi has overlapping bands close to the Brillouin zone center, making it a semimetal. The overlap arises from SOC; without the SOC the overlap would be removed and YPtBi would be a gapless semiconductor. The band overlap is not very strong, as indicated by the size of the Fermi surface. The surface consists of two hole pockets and two sets of electron pockets. The hole pockets are of approximately cubic shape centered around the zone center with corners along the  $\Lambda$  path. The inner hole pocket has a complex concave-convex shape and touches the outer hole pocket

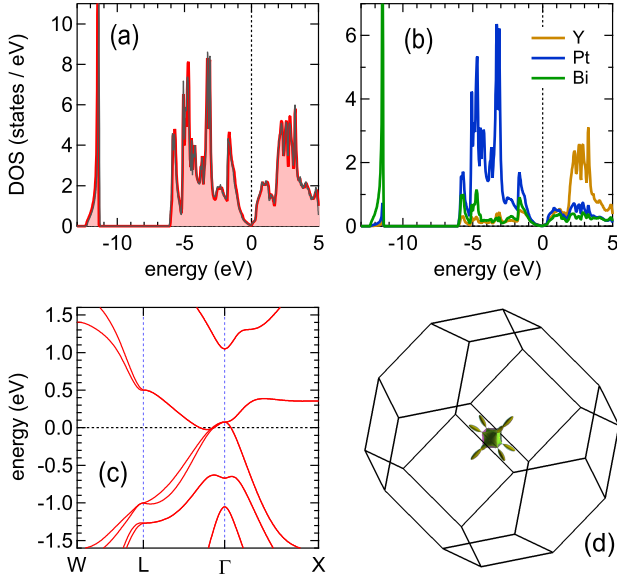


FIG. 2. (a) Density of states (DOS), (b) atom-projected density of states (PDOS), (c) band structure, and (d) Fermi surface of YPtBi obtained from FLAPW calculations. DOS plots obtained from the relativistic PAW (thin gray) and FLAPW (thick red) calculations are compared in (a) to show the equivalence of the two methods. The Fermi surface was obtained on a  $128^3$   $\mathbf{k}$ -point mesh. The outer electron and hole pockets are shown semitransparent.

on the  $\Lambda$  and  $\Delta$  paths. The electron pockets form a set of cigar-shaped ellipsoids with eightfold symmetry along the  $\Lambda$  paths. The small Fermi surface is in agreement with the small density of states at the Fermi energy of  $D(E_F) = 0.038$  states/eV. The calculated  $D(E_F)$  agrees very well with the value obtained from the heat capacity measurement,  $D(E_F) = 0.042$  states/eV [31].

The Fermi surface obtained for YPtBi is remarkably similar to the Fermi surface of LaPtBi [37]. The Fermi vector in [001] direction is  $k_F^{[001]} \approx 0.033 a_0^{-1}$  and the volume enclosed by the two hole pockets is approximately  $V_F^h \approx 0.000575 a_0^{-3}$ . The corresponding carrier density is  $n_e = n_h = 3 \cdot 10^{19} \text{ cm}^{-3}$ . Recently, Shubnikov-de Haas (SdH) oscillations in YPtBi single crystals with the magnetic field along the [001] direction were observed with a frequency of  $\Delta B^{-1} = 0.022 \text{ T}^{-1}$  [24], indicating that the true Fermi surface cross section is even three times smaller than the calculated one. For the latter, a frequency of SdH oscillations with a periodicity of  $\Delta B_{[001]}^{-1} \approx 0.0061 \text{ T}^{-1}$  is expected. Thus, the dip of the conduction band minimum below the valence band maximum on the  $\Lambda$  path is in fact not as deep as calculated. A beating node in the measurement indicates that there are two similar-sized Fermi surfaces contributing to the SdH oscillations, in perfect agreement with

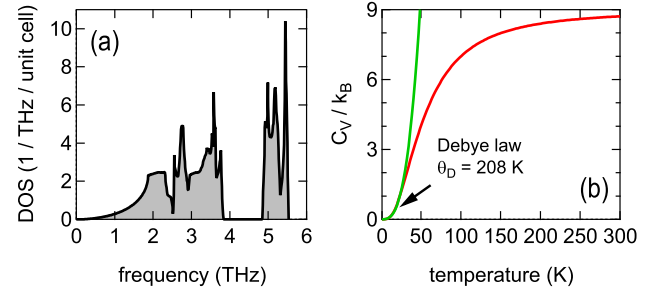


FIG. 3. Phonon density of states (a) and derived heat capacity (b) of pristine YPtBi.

the band structure calculation. Simultaneous Hall effect measurements were analyzed with a one-band model giving  $n_h = 2 \cdot 10^{18} \text{ cm}^{-3}$ . Based on the observed cross section of the Fermi surface and assuming cubic shape, one obtains an enclosed charge density of  $n_h \approx 4 \cdot 10^{18} \text{ cm}^{-3}$ , which agrees nicely with the Hall effect measurement, however neglecting multiband effects, different mobilities and carrier compensation. This result supports that the true Fermi surface is much smaller than the calculated one. The surface-averaged effective masses on the calculated Fermi surface are  $m_h^* = 0.2 m_e$  and  $m_e^* = 0.41 m_e$  for the hole and electron pockets, respectively, where  $m_e$  is the free-electron mass. The hole effective mass is roughly in agreement with the value extracted from SdH oscillation,  $m_h^* = 0.15 m_e$  [24]. The DFT electronic structure calculation reproduces the experimental observations very well up to a small error in the overlap between conduction and valence bands. Thus, the calculated electronic structure provides a solid foundation for the evaluation of the electron-phonon coupling discussed in the following.

The phonon density of states and heat capacity of YPtBi are shown in Figure 3. A clear separation of acoustic and optical modes is visible. From the low-temperature part of the heat capacity a Debye temperature of  $\Theta_D = 208 \text{ K}$  is obtained, in good agreement with the experimental value of  $195(5) \text{ K}$ . Because of the small Fermi surface, only very short  $\mathbf{q}$ -vectors with  $q \leq 2k_F$  can connect different parts of the surface, which gives rise to the scattering of an electron state into another. Thus, the electron-phonon coupling is limited to a small region close to the zone center. From the extrapolation scheme for the Brillouin zone integration  $\lambda = 0.02 \pm 0.02$  is obtained, obviously at the limit of the numerical accuracy of the Brillouin zone sampling. Certainly  $\lambda$  is small, but a more accurate  $\lambda$  will require an unfeasibly dense  $\mathbf{q}$ -point mesh. In pristine YPtBi the electron-phonon coupling constant  $\lambda$  is clearly much too small to explain the observed critical temperature of  $T_c = 0.77 \text{ K}$ , for which  $\lambda \geq 0.25$  is required, see Fig. 1.

To investigate the effect of doping, electron-phonon

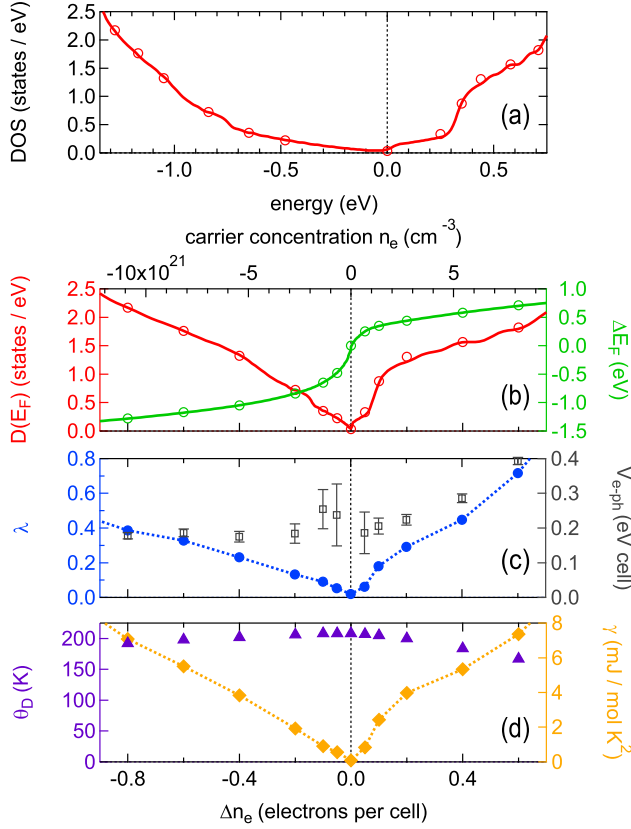


FIG. 4. (a) Density of states as a function of the energy. Open circles mark the values for which electron-phonon calculations were done. (b) Density of states and Fermi energy shift as a function of additional electrons per primitive cell  $\Delta n_e$ . (c) and (d) Electron-phonon coupling constant  $\lambda$ , interaction potential  $V_{e-ph} = \lambda/D(E_F)$ , Debye temperature  $\Theta_D$  and Sommerfeld coefficient  $\gamma$  as functions of  $\Delta n_e$ .

coupling was evaluated for doping levels of  $\Delta n_e = \pm 1.0$  electrons per primitive cell. The dynamical matrices were recomputed for each doping level, so that phonons were treated at full self-consistency with respect to doping. The corresponding densities of states and Fermi energy shifts are given in Fig. 4 (a) and (b). Because of the low DOS close to  $E_F$  in the undoped YPtBi, small doping levels already give rise to large Fermi energy shifts. With increasing doping of both electron- or hole-type, the electron-phonon coupling  $\lambda$  is increased as seen in Fig. 4 (c), however electron doping ( $\Delta n_e > 0$ ) is clearly more effective in increasing  $\lambda$ . The coupling leads to a renormalization of the phonon frequencies, which is indicated by the reduction of the Debye temperature, Fig. 4 (d). This also indicates that YPtBi could be dynamically unstable at strong doping. Coupling constants around  $\lambda \approx 0.25$  are obtained with  $\Delta n_e = +0.2$  or  $\Delta n_e = -0.4$ , which could give rise to a superconducting transition at the observed temperature of  $T_c = 0.77$  K, assuming  $\mu^* = 0$ . To study the influence of  $D(E_F)$  the electron-phonon in-

teraction potential  $V_{e-ph} = \lambda/D(E_F)$  is given in Fig. 4 (c). In the range  $\Delta n_e = \pm 0.2$  the interaction potential is  $V_{e-ph} \approx 0.22 \pm 0.03$  eV/cell, so the low value of  $\lambda$  for weakly and undoped YPtBi comes mainly from the low  $D(E_F)$ , or, equivalently, from the small Fermi surface area. These doping levels could be realized through off-stoichiometry (YPtBi crystals are mostly grown out of Bi flux, so additional Bi could easily be incorporated), or locally due to site-swap between neighboring cells. Also grain boundaries and other inhomogeneities with different stoichiometry could serve as sources of doping. The question that has to be answered in this context is, whether such doping is still consistent with other experimental data, for example the SdH oscillations or the heat capacity.

Doping levels of  $\Delta n_e = +0.2$  or  $\Delta n_e = -0.4$  correspond to carrier concentrations of  $n_e = 2.8 \times 10^{21} \text{ cm}^{-3}$  and  $n_h = 5.6 \times 10^{21} \text{ cm}^{-3}$ . These numbers are at least one order of magnitude larger than the typically observed carrier concentrations in YPtBi and three orders of magnitude larger than for the samples with lowest observed carrier concentration ( $2 \times 10^{18} \text{ cm}^{-3}$ , Ref. 24). Because of the increase in  $D(E_F)$  the Sommerfeld coefficient of the heat capacity,  $\gamma = \pi^2 D(E_F)(1+\lambda)k_B^2/3$  would increase to values around  $\gamma \approx 4 \text{ mJ/mol K}$ , see Fig. 4 (d). In both cases, the Fermi surface is enlarged and gets more complex, so that multiple high frequency SdH oscillations would be observed. However, experiments with high-quality samples indicate that the normal-state electronic properties of YPtBi are perfectly in agreement with the calculation for the ideal, undoped case [24, 25]. A diamagnetic screening fraction around 70% was observed in the superconducting state, underlining that a large part of the material is in the superconducting state and thereby ruling out the possibility of grain-boundary superconductivity [26]. Another remarkable observation is that the critical temperature of YPtBi varies little across different samples despite carrier concentrations and residual resistivities that vary over two orders of magnitude were found in these samples. From Eq. 1 one expects a very strong dependence of  $T_c$  on  $\lambda$ , so already small variations in the carrier concentration should lead to large changes in  $T_c$ . The lack of a clear correlation between normal-state electronic properties, sample quality, and critical temperature indicates that electron-phonon interaction induced by doping is not an explanation for the superconductivity in YPtBi. The relation between critical field and temperature observed in Ref. 25 deviates from conventional *s*-wave behavior and suggests that the material could be a *p*-wave superconductor, very similar to  $\text{Cu}_x\text{Bi}_2\text{Se}_3$ . On the other hand, Cooper pair wave functions with angular orbital momentum  $l > 0$  are not protected by the Anderson theorem, so random scattering from defects and impurities should reduce the ordering parameter and thereby  $T_c$  if the elastic mean-free-path  $\ell$  is smaller than the superconducting coherence length

$\xi$  [38]. Values of  $\xi = 15, 17$  nm and  $\ell = 105, 130$  nm were observed for YPtBi [24, 25], but superconductivity was also reported in a case where the mean free path based on free-electron theory, i.e.  $\ell = \hbar k_F / \rho_0 n e^2$  with  $k_F = (3\pi^2 n)^{1/3}$  is smaller than the lattice constant [9]. This indicates that YPtBi is superconducting even in the dirty limit. A remarkable side-note is that many Half-Heusler compounds are known as semiconductors that show large thermoelectric power at appropriate doping. Even though the carrier concentrations are often high, superconductivity has never been reported for any of these compounds [39].

Based on the analysis of the electron-phonon coupling obtained from first principles calculations and careful comparison with experimental data on the normal-state properties it is safe to conclude that an unconventional mechanism is responsible for the superconductivity in YPtBi. Related compounds from the class of topological Half-Heusler semimetals,  $RPtBi$  and  $RPdBi$  (with a rare-earth element  $R$ ) have very similar normal-state properties as YPtBi and also show superconductivity with critical temperatures up to 1.8 K. It is most likely that an unconventional pairing mechanism is at work in all of these compounds. More experimental work, in particular careful studies on the interplay between structural order, normal state electronic properties and superconductivity are necessary to gain more systematic knowledge about the pairing mechanism and the parity of the Cooper pairs. From the theoretical point of view it is particularly challenging to identify pairing mechanisms that allow for sufficiently strong coupling despite the low Fermi density of states, for example an electron-electron coupling assisted by plasmons [20].

Calculations leading to the results presented here were performed on resources provided by the Paderborn Center for Parallel Computing. The author thanks Thomas Dahm for fruitful discussions.

---

\* meinert@physik.uni-bielefeld.de

- [1] X.-L. Qi and S.-C. Zhang, Rev. Mod. Phys. 83, 1057 (2011).
- [2] H. Lin, L. A. Wray, Y. Xia, S. Xu, S. Jia, R. J. Cava, A. Bansil, and M. Z. Hasan, Nat. Mater. 9, 546 (2010).
- [3] W. Al-Sawai, H. Lin, R. S. Markiewicz, L. a. Wray, Y. Xia, S. Y. Xu, M. Z. Hasan, and A. Bansil, Phys. Rev. B 82, 125208 (2010).
- [4] W. Feng, D. Xiao, Y. Zhang, and Y. Yao, Phys. Rev. B 82, 235121 (2010).
- [5] C. Liu, Y. Lee, T. Kondo, E. D. Mun, M. Caudle, B. N. Harmon, S. L. Bud'Ko, P. C. Canfield, and A. Kaminski, Phys. Rev. B 83, 205133 (2011).
- [6] C. Shekhar, S. Ouardi, A. K. Nayak, G. H. Fecher, W. Schnelle, and C. Felser, Phys. Rev. B 86, 155314 (2012).
- [7] B. Nowak, O. Pavlosiuk, and D. Kaczorowski, J. Phys. Chem. C 119, 2770 (2015).
- [8] G. Goll, M. Marz, A. Hamann, T. Tomanic, K. Grube, T. Yoshino, and T. Takabatake, Physica B: Condens. Matt. 403, 1065 (2008).
- [9] C. Shekhar, M. Nicklas, A. K. Nayak, S. Ouardi, W. Schnelle, G. H. Fecher, C. Felser, and K. Kobayashi, J. Appl. Phys. 113, 17E142 (2013).
- [10] F. F. Tafti, T. Fujii, A. Juneau-Fecteau, S. Ren de Cotret, N. Doiron-Leyraud, A. Asamitsu, and L. Taillefer, Phys. Rev. B 87, 184504 (2013).
- [11] G. Xu, W. Wang, X. Zhang, Y. Du, E. Liu, S. Wang, G. Wu, Z. Liu, and X. X. Zhang, Sci. Rep. 4, 5709 (2014).
- [12] Y. Nakajima, R. Hu, K. Kirshenbaum, A. Hughes, P. Syers, X. Wang, K. Wang, R. Wang, S. R. Saha, D. Pratt, J. W. Lynn, and J. Paglione, Sci. Adv. 1500242 (2015).
- [13] M. Sigrist, D. F. Agterberg, P. A. Frigeri, N. Hayashi, R. P. Kaur, A. Koga, I. Milat, K. Wakabayashi, and Y. Yanase, J. Magn. Magn. Mater. 310, 536 (2007).
- [14] M. Sato and S. Fujimoto, Phys. Rev. B 79, 094504 (2009).
- [15] M. Leijnse and K. Flensberg, Semicond. Sci. Technol. 27, 124003 (2012).
- [16] R. A. Hein, J. W. Gibson, R. Mazelsky, R. C. Miller, and J. K. Hulm, Phys. Rev. Lett. 12, 320 (1964).
- [17] P. B. Allen and M. L. Cohen, Phys. Rev. 177, 704 (1969).
- [18] J. F. Schooley, W. R. Hosler, E. Ambler, J. H. Becker, M. L. Cohen, and C. S. Koonce, Phys. Rev. Lett. 14, 305 (1965).
- [19] E. Bustarret, Phys. C Supercond. Appl. 514, 36 (2015).
- [20] Y. Takada, J. Phys. Soc. Japan 49, 1267 (1980).
- [21] E. A. Ekimov, V. A. Sidorov, E. D. Bauer, N. N. Mel'nik, N. J. Curro, J. D. Thompson, and S. M. Stishov, Nature 428, 542 (2004).
- [22] Y. S. Hor, A. J. Williams, J. G. Checkelsky, P. Roushan, J. Seo, Q. Xu, H. W. Zandbergen, A. Yazdani, N. P. Ong, and R. J. Cava, Phys. Rev. Lett. 104, 057001 (2010).
- [23] X.-L. Zhang and W.-M. Liu, Sci. Rep. 5, 8964 (2015).
- [24] N. P. Butch, P. Syers, K. Kirshenbaum, A. P. Hope, and J. Paglione, Phys. Rev. B 84, 1 (2011).
- [25] T. V. Bay, T. Naka, Y. K. Huang, and A. de Visser, Phys. Rev. B 86, 1 (2012).
- [26] T. V. Bay, M. Jackson, C. Paulsen, C. Baines, A. Amato, T. Orvis, M. C. Aronson, Y. K. Huang, and A. de Visser, Solid State Commun. 183, 13 (2014).
- [27] P. Morel and P. W. Anderson, Phys. Rev. 125, 1263 (1962).
- [28] D. Y. Savrasov and S. Y. Savrasov, Phys. Rev. B 54, 16487 (1996).
- [29] A. Y. Liu and A. A. Quong, Phys. Rev. B 53, R7575 (1996).
- [30] A more accurate treatment is possible with the Allen-Dynes modified McMillan equation, which has a logarithmic averaged phonon frequency as input that is *a priori* unknown. See P. B. Allen and R. C. Dynes, Phys. Rev. B 12, 905 (1975) for details.
- [31] P. G. Pagliuso, C. Rettori, M. E. Torelli, G. B. Martins, Z. Fisk, J. L. Sarrao, M. F. Hundley, and S. B. Oseroff, Phys. Rev. B 60, 4176 (1999).
- [32] P. Giannozzi, S. Baroni, N. Bonini, M. Calandra, R. Car, C. Cavazzoni, D. Ceresoli, G. L. Chiarotti, M. Cococcioni, I. Dabo, A. Dal Corso, S. de Gironcoli, S. Fabris, G. Fratesi, R. Gebauer, U. Gerstmann, C. Gougousis, A. Kokalj, M. Lazzeri, L. Martin-Samos, N. Marzari, F. Mauri, R. Mazzarello, S. Paolini, A. Pasquarello, L. Paulatto, C. Sbraccia, S. Scandolo, G. Sclauzero, A. P. Seitsonen, A. Smogunov, P. Umari, and R. M. Wentzcov-

- itch, J. Phys. Condens. Matter 21, 395502 (2009).
- [33] A. Dal Corso, Phys. Rev. B 82, 075116 (2010).
  - [34] A. Dal Corso, Comp. Mat. Sci. 95, 337 (2014).
  - [35] <http://elk.sourceforge.net>
  - [36] M. Wierzbowska, S. de Gironcoli, P. Giannozzi, arXiv:cond-mat/0504077v2
  - [37] T. Oguchi, Phys. Rev. B **63**, 125115 (2001).
  - [38] A. P. Mackenzie and Y. Maeno, Rev. Mod. Phys. 75, 657 (2003).
  - [39] T. Graf, C. Felser, and S. S. P. Parkin, Prog. Solid State Chem. 39, 1 (2011).